European Radiology (2019) 29:889–897
https://doi.org/10.1007/s00330-018-5530-z

CHEST

Radiomics signature: a biomarker for the preoperative discrimination of lung invasive adenocarcinoma manifesting as a ground-glass nodule

Li Fan[1] · MengJie Fang[2,3] · ZhaoBin Li[4] · WenTing Tu[1] · ShengPing Wang[5] · WuFei Chen[6] · Jie Tian[2,3] · Di Dong[2,3] · ShiYuan Liu[1]

Received: 9 November 2017 / Revised: 3 April 2018 / Accepted: 7 May 2018 / Published online: 2 July 2018

Abstract

Objectives To identify the radiomics signature allowing preoperative discrimination of lung invasive adenocarcinomas from non-invasive lesions manifesting as ground-glass nodules.

Methods This retrospective primary cohort study included 160 pathologically confirmed lung adenocarcinomas. Radiomics features were extracted from preoperative non-contrast CT images to build a radiomics signature. The predictive performance and calibration of the radiomics signature were evaluated using intra-cross (n=76), external non-contrast-enhanced CT (n=75) and contrast-enhanced CT (n=84) validation cohorts. The performance of radiomics signature and CT morphological and quantitative indices were compared.

Results 355 three-dimensional radiomics features were extracted, and two features were identified as the best discriminators to build a radiomics signature. The radiomics signature showed a good ability to discriminate between invasive adenocarcinomas and non-invasive lesions with an accuracy of 86.3%, 90.8%, 84.0% and 88.1%, respectively, in the primary and validation cohorts. It remained an independent predictor after adjusting for traditional preoperative factors (odds ratio 1.87, $p < 0.001$) and demonstrated good calibration in all cohorts. It was a better independent predictor than CT morphology or mean CT value.

Conclusions The radiomics signature showed good predictive performance in discriminating between invasive adenocarcinomas and non-invasive lesions. Being a non-invasive biomarker, it could assist in determining therapeutic strategies for lung adenocarcinoma.

Key Points

- *The radiomics signature was a non-invasive biomarker of lung invasive adenocarcinoma.*
- *The radiomics signature outweighed CT morphological and quantitative indices.*
- *A three-centre study showed that radiomics signature had good predictive performance.*

Li Fan and MengJie Fang contributed equally to this work.

Electronic supplementary material The online version of this article (https://doi.org/10.1007/s00330-018-5530-z) contains supplementary material, which is available to authorized users.

✉ Di Dong
di.dong@ia.ac.cn

✉ ShiYuan Liu
lsy0930@163.com

[1] Department of Radiology, Changzheng Hospital, Second Military Medical University, No. 415 Fengyang Road, Shanghai 200003, China

[2] CAS Key Laboratory of Molecular Imaging, Institute of Automation, Chinese Academy of Sciences, No.95 Zhongguancun East Road, Beijing 100190, China

[3] University of Chinese Academy of Sciences, Beijing 100190, China

[4] Department of Radiation Oncology, The Sixth People's Hospital, Shanghai Jiaotong University, Shanghai 200233, China

[5] Department of Radiology, Fudan University Shanghai Cancer Center, Shanghai 200032, China

[6] Department of Radiology, Huadong Hospital Affiliated with Fudan University, Shanghai 200040, China

Keywords Lung · Adenocarcinoma · Tomography, x-ray computed · Computational biology · Solitary pulmonary nodule

Abbreviations

ANNs	Artificial neural networks
AUC	Area under the curve
CT	Computed tomography
DFS	Disease-free survival
GGN	Ground-glass nodule
GLCM	Grey-level co-occurrence matrix
GLRLM	Grey-level run-length matrix
IAC	Invasive adenocarcinoma
IASLC/ATS/ERS	International Association for the Study of Lung Cancer/American Thoracic Society/European Respiratory Society
LASSO	The least absolute shrinkage and selection operator
MIA	Minimally invasive adenocarcinoma
ROC	Receiver-operating characteristic

Introduction

Lung cancer is the leading cause of cancer-related mortality worldwide. Most early-stage lung cancers are adenocarcinomas and manifest as ground-glass nodules (GGNs) on thin-slice computed tomography (CT) [1]. Adenocarcinomas account for nearly 40% of all lung cancers [2, 3]. According to the classification system proposed by the International Association for the Study of Lung Cancer/American Thoracic Society/European Respiratory Society in 2011 [4], lung adenocarcinoma is classified into preinvasive adenocarcinoma (i.e., atypical adenomatous hyperplasia and adenocarcinoma in situ), minimally invasive adenocarcinoma (MIA) and invasive adenocarcinoma (IAC). Several studies have validated this new classification system, and the different subtypes of lung adenocarcinoma have different 3-year and 5-year disease-free survival rates [5–8]. The 5-year disease-free survival in adenocarcinoma in situ and MIA is 100%, which is significantly higher than that in IAC (range 38–86%, $p<0.001$), depending on the predominant histological subtype [7]. Some investigators consider adenocarcinoma in situ and MIA to be low-grade cancers because of their excellent prognosis and regard IAC as having intermediate or high-grade clinical behaviour [9]. The prognosis affects the clinical management of these tumours; for preinvasive adenocarcinoma or MIA, follow-up CT is recommended until the nodule diameter is > 1.5 cm or if the patient is aged older than 70 years [10]. In the future, patients with preinvasive adenocarcinoma or MIA may be candidates for limited surgical resection [9, 11].

Non-invasive differentiation of preinvasive adenocarcinoma or MIA from IAC preoperatively is essential to guide clinical management. The most common method used to make the differential diagnosis of lung nodules is based on morphology, such as lobulation and spiculation. In a previous study we found that morphological features on CT had high sensitivity (93.4%) and accuracy (86.6%) in the diagnosis of malignant GGN [12]. However, these GGNs have atypical features, so similar studies are rare [13]. Since 2011, certain quantitative parameters (e.g. the mean CT value and CT number histogram) have been helpful in making the differential diagnosis [14–16]. However, there is no consensus because of the variety of quantitative parameters available. Radiomics is an emerging field that converts imaging data into a high-dimensional mineable feature space using a large number of automatically extracted data characterisation algorithms [17]. Radiomics has been used in the prediction and prognosis of colorectal cancer, head and neck cancer, and lung cancer [18, 19]. Only few studies have used the radiomics signature on multiphase CT to discriminate between the subtypes of lung adenocarcinoma, particularly lung cancer manifesting as GGN. The aim of this three-centre study was to assess the ability of the radiomics signature to differentiate IAC of the lung from non-invasive lesions manifesting as GGNs.

Materials and methods

Patient population

The patient population in this retrospective multicentre study included a primary cohort and three validation cohorts (Fig. 1, Supplementary Material 1). The basic inclusion criteria for the primary and validation cohorts were as follows: a solitary malignant GGN without pleural or mediastinal adhesion diagnosed on multidetector CT, no previous treatment, a lesion manifesting as a GGN on thin-slice (< 1-mm) CT images, availability of complete thin-slice images reconstructed with a standard algorithm in Digital Imaging and Communications in Medicine (DICOM) format, and no marked cavity seen on thin-slice CT images. The exclusion criteria were multiple GGNs, pleural or mediastinal adhesions, previous treatment, incomplete thin-slice images reconstructed with a standard algorithm in DICOM format, and presence of a marked cavity. Preinvasive adenocarcinoma and MIA were considered to be non-invasive lesions.

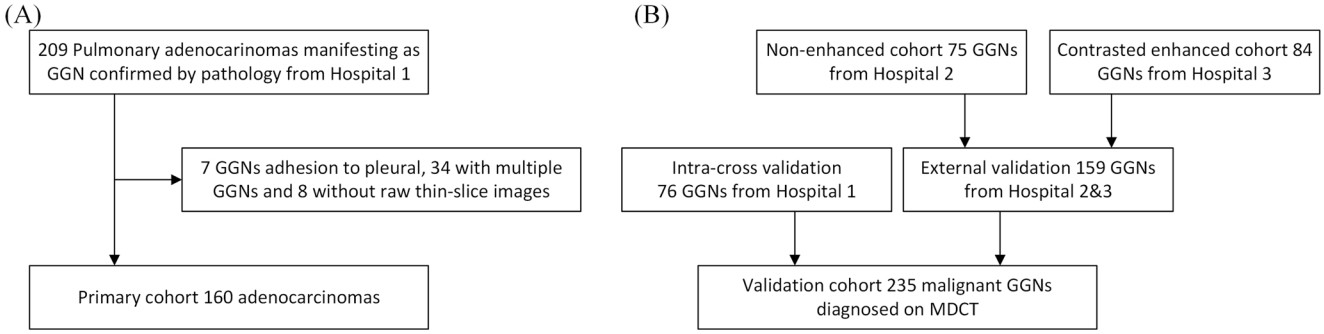

Fig. 1 The patient populations from the three centres. (**A**)Primary cohort, (**B**)validation cohorts, including an intra-cross validation cohort and two external validations

From November 2011 to October 2014, 209 consecutive patients with pulmonary adenocarcinoma confirmed by operative pathology to be manifesting as GGNs were admitted to hospital 1. Seven patients with GGNs with pleural adhesions, 34 with multiple GGNs, and eight with no raw thin-slice images available were excluded, leaving 160 patients (59 men, 101 women; age range, 27–80 years) with 160 GGNs for inclusion in the primary cohort. Seventy-seven patients in the primary cohort had non-invasive lesions and 83 had IAC. The demographic characteristics of the primary cohort and the three validation cohorts are summarised in Table 1. The study protocol was approved by the institutional review boards of the three participating hospitals. The need for informed patient consent was waived.

Image acquisition and segmentation

The imaging acquisition and segmentation methods used in the study are described in Supplementary Material 2. The reproducibility of intra-observer and inter-observer segmentation was confirmed by two experienced thoracic radiologists with 3 years and 13 years of experience.

CT morphology, mean CT value and building of a clinical model

All the thin-slice CT images were interpreted by two thoracic radiologists (with 13 years and 10 years of experience in chest CT) who were blinded to each subject's identity and clinical data. Decisions on CT findings were reached by consensus. The shape of the lesion was classified as 'irregular' or 'round/oval'. Marginal characteristics included lobulation, spiculation, cusp angle and spine-like process. The interfaces were classified into three types, i.e. ill-defined, well-defined and smooth, and well-defined but coarse. Internal characteristics included cystic changes, nodule sign, foam-like sign, vacuole sign and air bronchograms. Air bronchograms were reclassified as natural, dilated/distorted or cut-off. Findings in adjacent structures included the pleural indentation sign and vascular convergence sign. The mean CT value, a commonly used quantitative lung nodule parameter, was automatically calculated using a post-processing workstation after manual segmentation of the whole nodule. Starting with the statistically significant clinical characteristics, multivariable logistic regression analysis was used to build the clinical model as a simulation of the usual clinical decision-making process. Backward step-wise selection was

Table 1 Demographic characteristics of the patients in the four cohorts

Characteristic	Primary cohort (N = 160)	Intra-cross validation cohort (N = 76)	External validation cohort 1 (N = 75)	External validation cohort 2 (N = 84)
Sex (N)				
Men	59 (36.9%)	24 (31.6%)	29 (38.7%)	28 (33.3%)
Women	101 (63.1%)	52 (68.4%)	46 (61.3%)	56 (66.7%)
Age, y [median (IQR)]	57 (50–62)	56 (46–65)	59 (53–65)	56 (49–64)
Adenocarcinoma group (N)				
Noninvasive lesion	77 (48.1%)	36 (47.4%)	30 (40.0%)	49 (58.3%)
IAC	83 (51.9%)	40 (52.6%)	45 (60.0%)	35 (41.7%)

Note. External validation cohort 1 is the non-contrast-enhanced cohort; external validation cohort 2 is the contrast-enhanced cohort. No significant difference exists between the primary and validation cohorts for all demographic characteristics ($p > 0.05$)

IQR interquartile range

applied using the likelihood ratio test with Akaike's information criterion as the stopping rule.

Extraction and selection of radiomics features and building of the radiomics signature

The set of radiomics features used in this study contained 355 three-dimensional descriptors that are described in detail in Supplementary Material 3. The features were extracted using MATLAB 2014a (Mathworks, Natick, MA, USA). Selection of the radiomics features and building of the radiomics signature were based on the primary cohort. The least absolute shrinkage and selection operator (LASSO) method, which is suitable for regression of high-dimensional data, was used to obtain the most useful predictive combination of features to build the radiomics signature.

Evaluation of performance and statistical analysis

Unsupervised clustering and radiomic heatmaps were used to reveal clusters of patients with similar radiomic expression patterns, in which the association with the adenocarcinoma groups was evaluated. Univariate analysis was used to assess the relationship between patient characteristics and type of adenocarcinoma. Differences in variables between the patient groups were assessed using the independent *t*-test or Mann-Whitney *U* test for continuous variables and Fisher's exact test or chi-square test for categorical variables. The statistically significant clinical/morphological characteristics and the radiomic signature were used as the input variables for multivariable logistic regression analysis to identify independent predictors. Receiver-operating characteristic (ROC) curves were plotted for the study variables to assess their predictive performance and were compared using the Delong test. The area under the curve (AUC) of the ROC curve was obtained. The point on the ROC curve in the primary cohort at which the positive likelihood ratio was maximal was deemed to be the optimal cut-off threshold value and applied to the three validation cohorts. The accuracy of each predictor was then assessed using its sensitivity and specificity values. A curve was plotted to assess the calibration of the radiomic signature and accompanied by the Hosmer-Lemeshow test. Kappa tests were used to determine intra-reader and inter-reader agreement. Kappa values of 0.81–1.00 indicated very good agreement, 0.61–0.80 good agreement, and 0.41–0.60 moderate agreement.

The statistical analysis was performed using R software (version 3.0.1; R Foundation for Statistical Computing, Vienna, Austria; http://www.Rproject.org). A two-sided *p*-value < 0.05 was considered statistically significant.

Results

Demographic data, CT morphology and mean CT value

The demographic data, mean CT value and morphological features in the primary and validation cohorts are listed in Table 1 and Supplementary Table S1. There was no difference in sex, age or most morphological features between the group with non-invasive lesions and the group with IAC in the primary or validation cohorts ($p > 0.05$). There were significant differences in the mean CT value, lobulation, spiculation, spine-like process, air bronchogram and pleural indentation rates between the two groups. The cut-off mean CT value was -516 Hounsfield units (HU).

Backward step-wise selection was used to build the clinical model and showed that the mean CT value, lobulation, foam-like sign, vacuole sign and pleural indentation were important indicators of IAC. The corresponding regression equation was as follows:

$$\begin{aligned}\mathrm{In}(\mathrm{P}/1-\mathrm{P}) = {} & -2.830 + 0.008 \times \text{mean CT value} + 1.065 \\ & \times \text{lobulation} - 0.756 \times \text{foam}-\text{likesign} - 0.666 \\ & \times \text{vacuolesign} + 1.238 \times \text{pleural indentation}\end{aligned}$$

in which P is the probability of IAC. For $p \geq 0.5$, the lesion was expected to be IAC, while the other lesions were categorised as non-invasive lesions.

Extraction and selection of radiomics features and building of the radiomics signature

After assessing the reproducibility based on the re-segmentation data and evaluating the differentiating ability of the radiomics features in univariate analysis, 254 features with intraclass correlation coefficients > 0.75 and *p*-values < 0.05 were selected. Based on the heatmap, two main clusters of patients were compared and a significant association was found, demonstrating the potential discriminative power of these radiomics features (Fig. 2). After removing features that were strongly correlated (i.e. with a correlation coefficient > 0.6), 28 robust imaging features remained. These features were reduced to two potential predictors (1_GLCM_correlation and 0_GLCM_cluster_tendency; Supplementary Table S2), that had non-zero coefficients in the LASSO logistic regression model in the primary cohort (Supplementary Fig. S1). These features were included in the calculation formula for the radiomics signature as follows:

$$\begin{aligned}\text{signature score} = {} & 2.307 + 4.995 \\ & \times \text{1\_GLCM\_correlation} - 7.660 \\ & \times \text{0\_GLCM\_cluster\_tendency}\end{aligned}$$

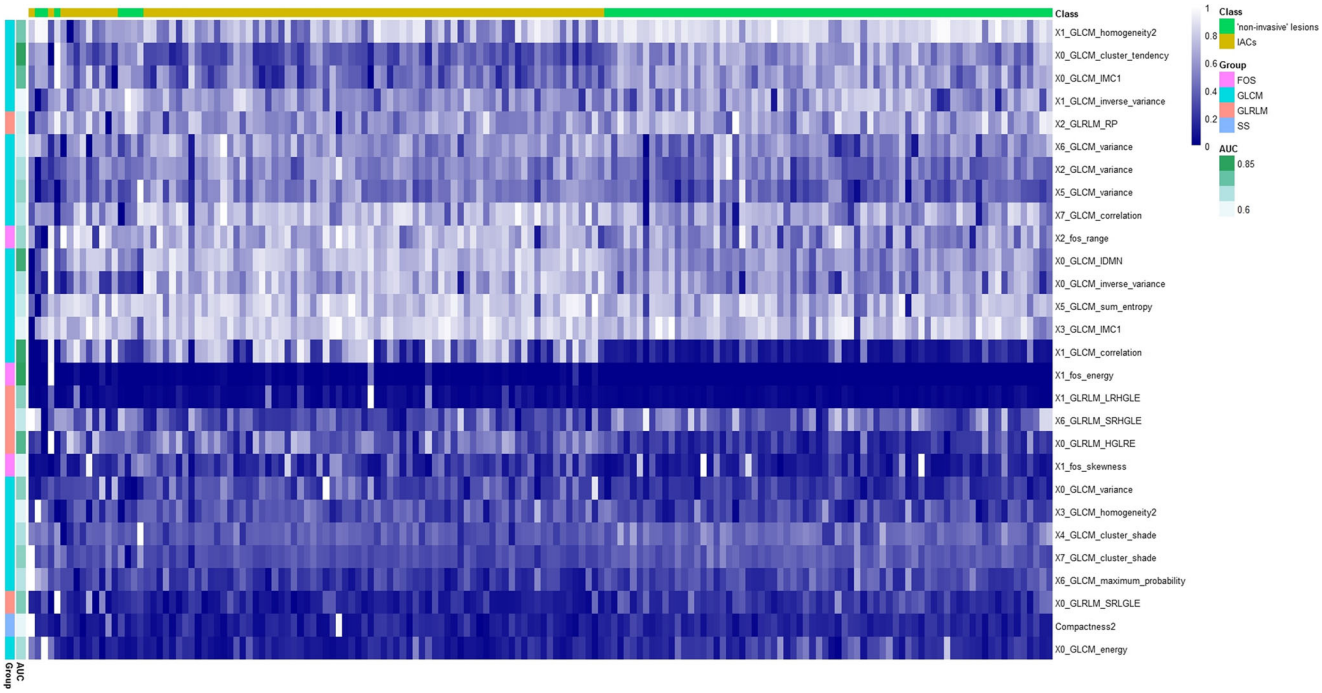

Fig. 2 Radiomics heatmap of the significant features. Unsupervised clustering of patients (n=160) on the y-axis and expression of radiomics features (n=28) on the x-axis reveal clusters of patients with similar radiomic expression patterns. There is a significant association of the radiomics feature expression patterns with the two groups of GGN. The groups and the AUC of these radiomics features are labelled on the left side

Predictive performance and validation of the radiomics signature

The radiomics signature showed good performance for discriminating between non-invasive lesions and IACs in the primary and validation cohorts (Table 2, Fig. 3). The optimal cut-off threshold value for the radiomics signature was 0.519. There was a significant difference in the radiomics signature between the two groups ($p < 0.001$). Furthermore, stratified analysis showed that the radiomics signature remained statistically significant after adjustment for age and sex (Supplementary Table S3).

The calibration curve of the radiomics signature for the predicted risk of IAC demonstrated good agreement between prediction and observation in all cohorts (Supplementary Material 4, Fig. S2).

Comparison of the predictive performance of the radiomics signature with that of the clinical characteristics

The AUC of the ROC curves (Fig. 3) for the statistically significant characteristics and the clinical model were calculated and compared with those of the radiomics signature using the Delong test (Table 3). There were significant differences between the AUC for the radiomics signature and those for all other predictors ($p < 0.05$). Therefore, the radiomics signature had the best discriminative performance of all the

Table 2 Predictive performance of the radiomics signature in the primary and validation cohorts

Cohorts	Signature score [median (IQR)]		AUC (95% CI)	Accuracy	Sensitivity	Specificity
	Noninvasive lesion	IAC				
Primary cohort	0.163 (0.065–0.355)	0.929 (0.678–0.985)	0.917 (0.874–0.959)	86.3%	83.1%	89.6%
Intra-cross validation cohort	0.093 (0.054–0.165)	0.957 (0.711–0.994)	0.971 (0.942–1.000)	90.8%	87.5%	94.4%
External validation cohort 1	0.170 (0.063–0.301)	0.849 (0.561–0.966)	0.942 (0.895–0.989)	84.0%	82.2%	86.7%
External validation cohort 2	0.057 (0.027–0.211)	0.869 (0.619–0.969)	0.936 (0.887–0.986)	88.1%	85.7%	89.8%

Note. External validation cohort 1 is the non-contrast-enhanced cohort. External validation cohort 2 is the contrast-enhanced cohort

IQR interquartile range

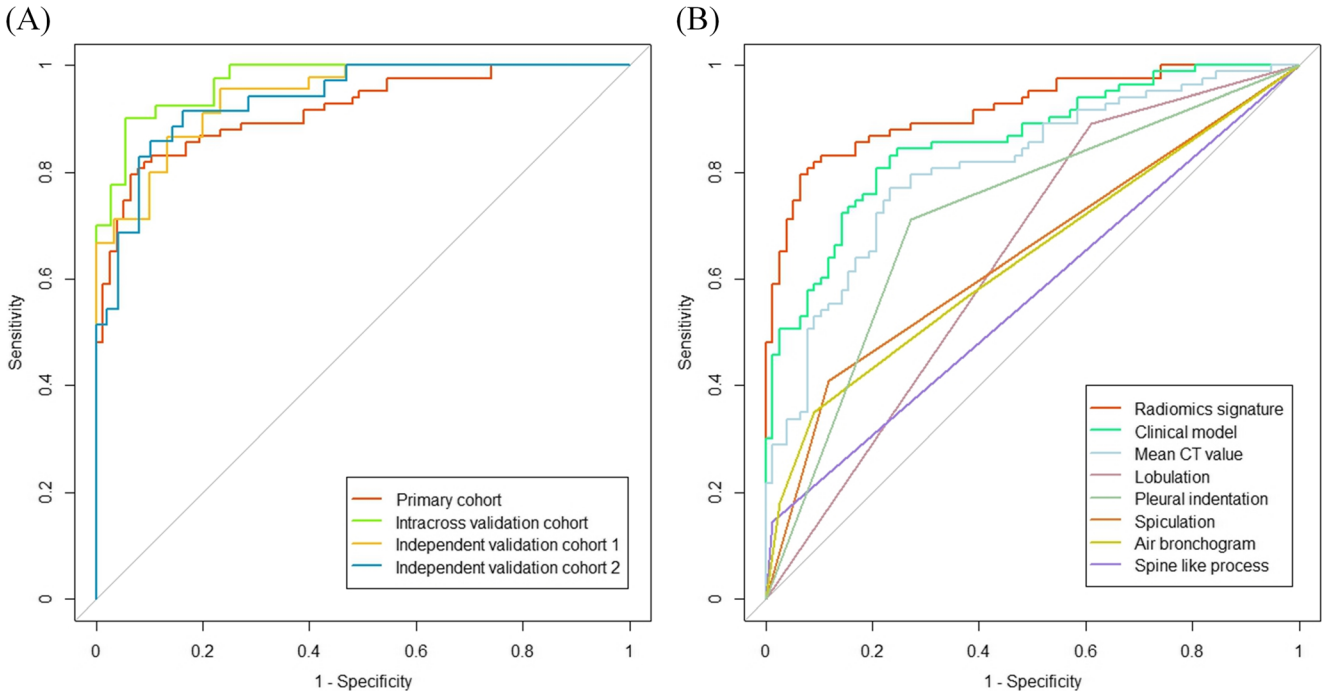

Fig. 3 Results of the receiver-operating characteristic (ROC) curve analysis. (**A**) The ROC curves for the radiomics signature in the four cohorts. (**B**) The ROC curves for the radiomics signature, clinical model and six clinical characteristics in the primary cohort

characteristics. Multivariate logistic regression analysis also revealed that the radiomics signature was the only independent predictor (Table 4).

Discussion

We built a radiomics signature based on two radiomics features to discriminate non-invasive adenocarcinoma from IAC and validated this signature in multicentre cohorts. The radiomics signature had the best discriminative performance when compared with the most commonly used clinical parameters, such as mean CT value and morphological features.

Table 3 The areas under the curve for six characteristics and clinical model and comparison with the radiomics signature

Characteristic	AUC (95% CI)	*p*-value
Mean CT value	0.808 (0.741–0.875)	< 0.001*
Lobulation	0.641 (0.576–0.705)	< 0.001*
Spiculation	0.646 (0.582–0.711)	< 0.001*
Spine-like process	0.566 (0.526–0.606)	< 0.001*
Air bronchogram	0.639 (0.561–0.717)	< 0.001*
Pleural indentation	0.719 (0.649–0.789)	< 0.001*
Clinical model	0.857 (0.801–0.914)	0.005*

*Indicates *p*-value < 0.05.

Moreover, the AUC was greater in each of the external validation cohorts, suggesting that the radiomics signature is a convenient and non-invasive biomarker of the risk of IAC.

The morphological features on CT and the mean CT value are the methods most commonly used in routine clinical practice for the differential diagnosis. A GGN with lobulation, a well-defined but coarse interface and pleural indentation has a greater-than-average likelihood of being malignant in view of the high sensitivity (93.4%) and accuracy (86.6%) of these features [12]. Accordingly, cancerous lesions were diagnosed in all our validation cohorts on multidetector CT, and the diagnoses were later confirmed pathologically. The features of early-stage lung cancer are usually atypical, which makes the differential diagnosis of the adenocarcinoma subtypes more difficult. Univariate analysis revealed no difference in most features between IAC and a non-invasive lesion. However, the clinical model included lobulation, pleural indentation, the foam-like sign, the vacuole sign and the mean CT value. Morphology has a prominent role in the clinical setting, but its worth may depend on the radiologist's experience and ability to recognise the signs, which may well explain why the AUC for morphological characteristics was lower than that for the radiomics signature in our study.

A number of studies have found that quantitative imaging can identify the pathological invasiveness of lung adenocarcinomas [16, 20, 21]. The most common quantitative indicators used to date have been the mean CT value and CT number histogram. Pure GGNs with a maximum diameter of ≤ 10 mm

Table 4 Results of multivariate logistic regression analysis

Variables	β	Adjusted OR (95% CI)	*p*-value
Mean_CT value (per 100 increase)	-0.06	0.94 (0.57-1.54)	0.798
Lobulation (no vs. yes)	-0.26	0.77 (0.24-2.52)	0.667
Spiculation (no vs. yes)	-0.69	0.50 (0.13-1.99)	0.327
Spine-like process (no vs. yes)	1.37	3.95 (0.10-157.31)	0.465
Air bronchogram (no vs. yes)	-0.04	0.96 (0.57-1.61)	0.878
Pleural indentation (no vs. yes)	0.68	1.98 (0.70-5.54)	0.196
Radiomic signature (per 0.1 increase)	0.63	1.87 (1.46-2.40)	< 0.001

and a CT value of -600 HU or lower are nearly always preinvasive lesions [22]. The cut-off for the mean CT value in the present study was -516 HU, which is slightly higher than -600 HU and may reflect use of different classifications. In our study, MIA and preinvasive lesions were considered to be non-invasive because of their good prognosis, which can reflect a high mean CT value. Lim et al [23] demonstrated that the mean CT value for IAC was -507 HU, which is very similar to our finding. Table 3 shows that the discriminative performance of the mean CT value is similar to that of a clinical model but inferior to the radiomics signature ($p < 0.05$). Nomori et al [24] and Ikeda et al [15] analysed the histograms of two-dimensional and three-dimensional CT pixel numbers, respectively, and found that the CT number-based histographic pattern was useful in differentiating atypical adenomatous hyperplasia from bronchioloalveolar carcinoma. In the present study, a three-dimensional histogram was used to discriminate non-invasive lesions from IACs using an alternative predictor known as 'first-order statistical features' and nearly all of them were significantly different between the two sorts ($p < 0.001$) and showed excellent inter-reproducibility and intra-reproducibility agreement (intraclass correlation coefficient > 0.75).

In recent years, it has been suggested that radiomics methods are advanced computational methodologies that can be applied to medical imaging data to convert medical images into quantitative descriptors of cancerous tissue [25, 26]. Coroller et al [27] evaluated CT radiomic features for their ability to predict distant metastasis in patients with lung adenocarcinoma and found that 35 radiomic features were prognostic (confidence interval > 0.60; false discovery rate < 5%) for distant metastasis and 12 for survival. Chae et al [28] used three-layered artificial neural networks with a back-propagation algorithm to build a discriminating model and found that the model had good power for differentiation of preinvasive lesions from invasive pulmonary adenocarcinomas with five input units, which were the first-order statistical features used in our study. However, their study included only 22 features (few of which were texture features) and there was no comprehensive analysis. Therefore, the role of a large number of radiomics features in this target has not been investigated thoroughly in previous studies. In this study, 355 radiomics features were analysed and a large number of robust radiomics features showed considerable potential for discriminating between IACs and non-invasive lesions manifesting as GGNs. The artificial neural network is a helpful tool to use for the problem of binary classification; however, there are always obstacles to broad application of any given model because of the complicated structure and parameters involved and the subsequent potential over-fitting problem.

In our study, the radiomics signature demonstrated excellent discrimination in all three validation cohorts (with respective AUCs of 0.971, 0.942 and 0.936), which surprisingly showed improvement when compared with the primary cohort (AUC 0.917). The contrast-enhanced CT images were also set as the validation cohort. Contrast-enhanced CT would not affect the display or the evaluation of morphological features, and only the mean CT value would increase. The mean CT value for IAC in the contrast-enhanced validation cohort was -398.1 ± 161.3 HU, which was significantly higher than the value for the non-contrast-enhanced validations. Most IACs manifested as mixed GGNs containing solid components with an increased blood supply. However, an increased CT value might not have affected the radiomics signature because the two selected radiomics features were both quantitative indicators measuring the degree of dispersion of the GLCMs from different aspects. The deviation of the matrix from its mean in the two indicators could be a process of calibration that reduced the effect of the whole increase in image intensity, thereby implying that the radiomics signature may be independent of the injection of a contrast agent. Improved discrimination implies that this signature is robust for prediction and could be applied directly in the validation cohort, omitting the process of adjusting the intercept and regression coefficients with regard to signature building.

The radiomics signature was robust and repeatable. At present, if a GGN is diagnosed as malignant according to its morphological features on CT, the nodule is segmented manually. Based on the original CT image and the segmentation result, the radiomics signature is then calculated as the probability risk of IAC by our scoring system automatically within 15 s. Our team [29, 30] is developing a method for automatic segmentation of lung nodules, and the raw CT data and automatic segmentation of a lung nodule will be integrated in the

near future, allowing the probability risk of an IAC to be outputted automatically. This method would have great potential in terms of personalised medicine.

This study has some limitations: First is its retrospective nature and potential bias. Second, the radiomics features were derived from the results of manual segmentation. Small internal vessels and the bronchi could not be excluded, which would have affected the accuracy of some features. Three-dimensional tumour segmentation is a complex and time-consuming process. Therefore, a reliable and robust automatic boundary extraction method needs to be used to address the variability issue.

In conclusion, the radiomics signature can provide a robust, non-invasive, low-cost and repeatable method for preoperative differentiation of IACs from non-invasive lesions. In the near future, the raw CT data and automatic segmentation of lung nodules will be able to be integrated, allowing the probability risk of IAC to be outputted automatically and potentially hasten the development of personalised medicine.

Funding This study has received funding by the National Natural Science Foundation of China (grant numbers 81370035, 81230030, and 81771924), The National Key R&D Program of China (grant number 2016YFE0103000, 2017YFC1308703, 2017YFA0205200, 2017YFC1309100 and 2017YFC1308700), Shanghai Pujiang Talent Program (grant number 15PJD002).

Compliance with ethical standards

Guarantor The scientific guarantor of this publication is Prof. Shiyuan Liu.

Conflict of interest The authors of this article declare no relationships with any companies whose products or services may be related to the subject matter of the article.

Statistics and biometry One of the authors has significant statistical expertise.

Informed consent Written informed consent was waived by the Institutional Review Board.

Ethical approval Institutional Review Board approval was obtained.

Methodology
- retrospective
- diagnostic or prognostic study
- multicentre study

References

1. Goo JM, Park CM, Lee HJ (2011) Ground-glass nodules on chest CT as imaging biomarkers in the management of lung adenocarcinoma. AJR Am J Roentgenol 196:533–543
2. Siegel R, Naishadham D, Jemal A (2013) Cancer statistics. CA Cancer J Clin 63:11–30
3. de Groot P, Munden RF (2012) Lung cancer epidemiology, risk factors, and prevention. Radiol Clin North Am 50:863–876
4. Travis WD, Brambilla E, Noguchi M et al (2011) International Association for the Study of Lung Cancer/American Thoracic Society/European Respiratory Society international multidisciplinary classification of lung adenocarcinoma. J Thorac Oncol 6:244–285
5. Russell PA, Wainer Z, Wright GM et al (2011) Does lung adenocarcinoma subtype predict patient survival? A clinicopathologic study based on the new International Association for the Study of Lung Cancer/American Thoracic Society/European Respiratory Society international multidisciplinary lung adenocarcinoma classification. J Thorac Oncol 6:1496–1504
6. Luo J, Huang Q, Wang R et al (2016) Prognostic and predictive value of the novel classification of lung adenocarcinoma in patients with stage IB. J Cancer Res Clin Oncol 142:2031–2040
7. Yanagawa N, Shiono S, Abiko M et al (2013) New IASLC/ATS/ERS classification and invasive tumor size are predictive of disease recurrence in stage I lung adenocarcinoma. J Thorac Oncol 8:612–618
8. Yoshiya T, Mimae T, Tsutani Y et al (2016) Prognostic role of subtype classification in small-sized pathologic N0 invasive lung adenocarcinoma. Ann Thorac Surg 102:1668–1673
9. Yoshizawa A, Motoi N, Riely GJ et al (2011) Impact of proposed IASLC/ATS/ERS classification of lung adenocarcinoma: prognostic subgroups and implications for further revision of staging based on analysis of 514 stage I cases. Mod Pathol 24:653–664
10. Lee HY, Choi YL, Lee KS et al (2014) Pure ground-glass opacity neoplastic lung nodules: histopathology, imaging, and management. AJR Am J Roentgenol 202:W224–W233
11. Ding H, Shi J, Zhou X et al (2017) Value of CT characteristics in predicting invasiveness of adenocarcinoma presented as pulmonary ground-glass nodules. Thorac Cardiovasc Surg 65:136–141
12. Fan L, Liu SY, Li QC et al (2012) Multidetector CT features of pulmonary focal ground-glass opacity: differences between benign and malignant. Br J Radiol 85:897–904
13. Zhang Y, Qiang JW, Shen Y et al (2016) Using air bronchograms on multi-detector CT to predict the invasiveness of small lung adenocarcinoma. Eur J Radiol 85:571–577
14. Shikuma K, Menju T, Chen F et al (2016) Is volumetric 3-dimensional computed tomography useful to predict histological tumour invasiveness? Analysis of 211 lesions of cT1N0M0 lung adenocarcinoma. Interact Cardiovasc Thorac Surg 22:831–838
15. Ikeda K, Awai K, Mori T et al (2007) Differential diagnosis of ground-glass opacity nodules: CT number analysis by three-dimensional computerized quantification. Chest 132:984–990
16. Yu WS, Hong SR, Lee JG et al (2016) Three-dimensional ground glass opacity ratio in C T images can predict tumor invasiveness of stage Ia lung cancer. Yonsei Med J 57:1131–1138
17. Aerts HJ, Velazquez ER, Leijenaar RT et al (2014) Decoding tumour phenotype by noninvasive imaging using a quantitative radiomics approach. Nat Commun 5:4006
18. Parmar C, Leijenaar RT, Grossmann P et al (2015) Radiomic feature clusters and prognostic signatures specific for lung and head and neck cancer. Sci Rep 5:11044
19. Huang YQ, Liang CH, He L et al (2016) Development and validation of a radiomics nomogram for preoperative prediction of lymph node metastasis in colorectal cancer. J Clin Oncol 34:2157–2164
20. Sakakura N, Inaba Y, Yatabe Y et al (2016) Estimation of the pathological invasive size of pulmonary adenocarcinoma using high-resolution computed tomography of the chest: a consideration based on lung and mediastinal window settings. Lung Cancer 95:51–56
21. Son JY, Lee HY, Kim JH et al (2016) Quantitative CT analysis of pulmonary ground-glass opacity nodules for distinguishing invasive adenocarcinoma from non–invasive or minimally invasive adenocarcinoma: the added value of using iodine mapping. Eur Radiol 26:43–54

22. Kitami A, Sano F, Hayashi S et al (2016) Correlation between histological invasiveness and the computed tomography value in pure ground-glass nodules. Surg Today 46:593–598
23. Lim HJ, Ahn S, Lee KS et al (2013) Persistent pure ground glass opacity lung nodules ≥10 mm in diameter at CT scan: histopathologic comparisons and prognostic implications. Chest 144:1291–1299
24. Nomori H, Ohtsuka T, Naruke T et al (2003) Differentiating between atypical adenomatous hyperplasia and bronchioloalveolar carcinoma using the computed tomography number histogram. Ann Thorac Surg 76:867–871
25. Kumar V, Gu Y, Basu S et al (2012) Radiomics: the process and the challenges. Magn Reson Imaging 30:1234–1248
26. Zhao B, Tan Y, Tsai WY et al (2016) Reproducibility of radiomics for deciphering tumor phenotype with imaging. Sci Rep 6:23428
27. Coroller TP, Grossmann P, Hou Y et al (2015) CT-based radiomic signature predicts distant metastasis in lung adenocarcinoma. Radiother Oncol 114:345–350
28. Chae HD, Park CM, Park SJ et al (2014) Computerized texture analysis of persistent part-solid ground-glass nodules: differentiation of preinvasive lesions from invasive pulmonary adenocarcinomas. Radiology 273:285–293
29. Song J, Yang C, Fan L et al (2016) Lung lesion extraction using a toboggan based growing automatic segmentation approach. IEEE Trans Med Imaging 35:337–353
30. Wang S, Zhou M, Liu Z et al (2017) Central focused convolutional neural networks: Developing a data-driven model for lung nodule segmentation. Med Image Anal 40:172–183